Environmental Earth Sciences (2018) 77:262
https://doi.org/10.1007/s12665-018-7438-y

ORIGINAL ARTICLE

An updated review about carbon dioxide and climate change

Rex J. Fleming[1]

Received: 18 December 2017 / Accepted: 20 March 2018 / Published online: 27 March 2018

Abstract

This manuscript will review the essence of the role of CO_2 in the Earth's atmosphere. The logic of CO_2 involvement in changing the climate will be investigated from every perspective: reviewing the historical data record, examining in further detail the twentieth-century data record, and evaluating the radiation role of CO_2 in the atmosphere—calculating and integrating the Schwarzschild radiation equation with a full complement of CO_2 absorption coefficients. A review of the new theory of climate change—due to the Sun's magnetic field interacting with cosmic rays, is provided. The application of this new theory is applied to climate-change events within the latter part of the Earth's interglacial period. The application to the Earth's Ice Ages is not detailed here due to manuscript size constraints, but is referenced for the reader. The results of this review point to the extreme value of CO_2 to all life forms, but no role of CO_2 in any significant change of the Earth's climate.

Keywords Carbon dioxide · Climate change · Solar magnetic field · Cosmic rays · Chaos

Introduction

The climate of planet Earth involves many nonlinear processes of the atmosphere, ocean, and other Earth sciences. This document will review what is known about these processes and explain an unfortunate misconception about *climate change*.

A specific definition of *climate change* is used to separate the term from the tremendous diversity of weather conditions that prevail on Earth. *Climate change* here implies the average surface temperature of the Earth adjusting upward or downward over a multi-year period (> 10-year). A significant external force is required to make such a change, e.g., a significant change in a solar property and/or a change in the Earth's albedo (the measure of how much the Sun's energy is reflected back into space).

Many believe and/or support the notion that the Earth's atmosphere is a "greenhouse" with CO_2 as the primary "greenhouse" gas warming Earth. That this concept seems acceptable is understandable—the modern heating of the Earth's atmosphere began at the end of the Little Ice Age in 1850. The industrial revolution took hold about the same time. It would be natural to believe that these two events could be the reason for the rise in temperature. There is now a much clearer picture of an alternative reason for why the Earth's surface temperature has risen since 1850.

There is a thermal blanket or buffer for atmospheric surface conditions that have been in existence for the past billion years—existing in all "*climate-change regimes*" (warm or cold). Its exact form depends on the effective solar energy reaching the Earth's surface. The sources of the thermal blanket and the subsequent transfer of heat upward are from three forces: the Earth's gravitational field with its impact on convection, the condensation of water vapor (H_2O), and the radiation effects of the two primary atmospheric trace gases of H_2O and CO_2. It will be demonstrated that the radiative roles of H_2O and CO_2 are relatively minor, compared to their far more important role in maintaining sustained life on our planet.

The purpose here is to objectively examine every facet of the CO_2/climate-change issue. This will entail a review of the historical record of *climate change* and that of the twentieth-century warming relative to CO_2 concentrations. The appropriate radiation code for the Earth's atmosphere will be examined in far more detail than is typically exposed in the scientific literature.

"The atmosphere and its extremely diverse weather" section describes the Earth's chaotic atmosphere and the diversity of the weather produced. This chaotic weather

✉ Rex J. Fleming
rex@rexfleming.com

1 Global Aerospace, LLC, 7225 Spring Drive, Boulder, CO 80303, USA

variability will continue to exist within each *climate-change regime*. "Does CO_2 have a role in causing climate change? Observations examined" section reviews the early evolution of the atmosphere, and the ice ages of the past through the current modest ice age. Within ice ages, there are *glacial periods* with ice sheets and *interglacial periods* with little or no ice. Two different proposed reasons for the twentieth-century warming are examined.

Fourth section explains "The source of the Earth's thermal blanket". This daily recurring thermal protective layer, and the subsequent immediate heat transfer upward occur due to the three physical causes. These forces act to create a balance between the incoming solar shortwave and outgoing longwave energy.

"H_2O and CO_2 in the radiation package" section quantifies the radiation roles of H_2O and CO_2. The standard approach to the radiation transfer is used—the integration of the Schwarzschild equation. "Solar magnetic field/cosmic ray factors affecting climate change" section summarizes the factors that cause *climate change* in the new theory of the interaction of the Sun's magnetic field with cosmic rays. "Summary" section provides a very brief review of the benefits of this important molecule, and a summary.

The atmosphere and its extremely diverse weather

The atmosphere has a temperature profile which decreases with height through the troposphere which contains 80% of its mass. At the minimum temperature level of the troposphere is the tropopause—this varies with latitude and season. The tropopause height is generally 9 km over the poles and 16–17 km at the equator.

Above the tropopause is the stratosphere where temperature increases with height to about 50 km. The stratosphere obtains its heat by the direct absorption of the Sun's energy by ozone (O_3).

The primary driver of Earth's weather systems is the very large-scale process of baroclinic instability that occurs independently in both hemispheres. Differential heating between the incoming solar radiation and the outgoing infrared radiation creates a pole-to equator temperature gradient and produces a growing supply of available potential energy. Eventually, the zonal thermal wind, developing to balance that temperature gradient, becomes baroclinically unstable. The resulting large-scale baroclinic waves transfer warm air poleward and cold air equatorward.

At the same time, the *eddy* (wave) available potential energy is converted into eddy kinetic energy by the vertical motion within the waves—maintaining the kinetic energy of the atmosphere against frictional dissipation. The waves intensify until the heat transferred poleward balances the radiation deficit. Various processes within the atmosphere (friction, radiation to space, etc.) damp the unstable waves and the baroclinic cycle is repeated.

Thompson (1987) developed a low-order general circulation model consisting of a single finite amplitude baroclinic wave interacting with the zonal mean shear flow, maintained against a friction parameter (**D**) and driven by a differential heating term (**H**)—thus containing all the requirements for baroclinic instability. The model produced accurate values for certain features including the *vacillation period* [the time from a zonal flow (non-wave) configuration to the maximum wave development, and back again to zonal flow] of approximately 23 days—close to that seen in the Southern Hemisphere (Webster and Keller 1975).

Vacillation, with fixed point attractors, were the only dynamic entities included and described in Thompson's original presentation. Later this model was found to produce two other attractor types: limit cycles and chaos (Fleming 2014). The chaos was produced over various values of the parameters **D** and **H**, and also produced by the process of sensitivity to the initial conditions—whereby on a strange attractor two initially close trajectories on the attractor eventually diverge from one another—exponentially over time.

The variability of the simple model above will be demonstrated, but this diversity would have been more intense with the 4–6 waves included (typically seen in a hemisphere) allowing wave–wave nonlinear interaction.

Figure 1 (Fleming 2014) indicates two solutions in the above model, vacillation, and chaos, respectively, where $X(1)$ represents the mean horizontal temperature gradient and $X(2)$ represents the net poleward heat transport. The longest vacillation cycle was 25.2 days. The longest chaos cycle was 35.0 days. The initial conditions were the same for all the parameters and variables—except that the initial mean horizontal temperature gradient [$X(1)$] was 67% of its fixed point value for the vacillation solution, and 66% of that value for the chaos solution.

Notice the significant difference in the scales of the two solutions in Fig. 1. The important difference between vacillation and chaos is that the range of $X(1)$ and $X(2)$ is approximately three times greater for the chaos case—the complete trajectory of the vacillation solution nearly fits inside the opening in the chaos trajectory. When such a large solution difference occurs from such two closely spaced initial points, this is explosive baroclinic instability (EBI).

A Monte Carlo approach evaluated the power of the chaos within this nonlinear model of baroclinic instability. Using a known chaos initial state for $X(1)$, 40,000 different initial states were selected from a random number generator for a normal distribution with a standard deviation of only 0.001. The only model value changed for the 40,000 different deterministic runs was $X(1) = 0.4 +$ the normal deviate.

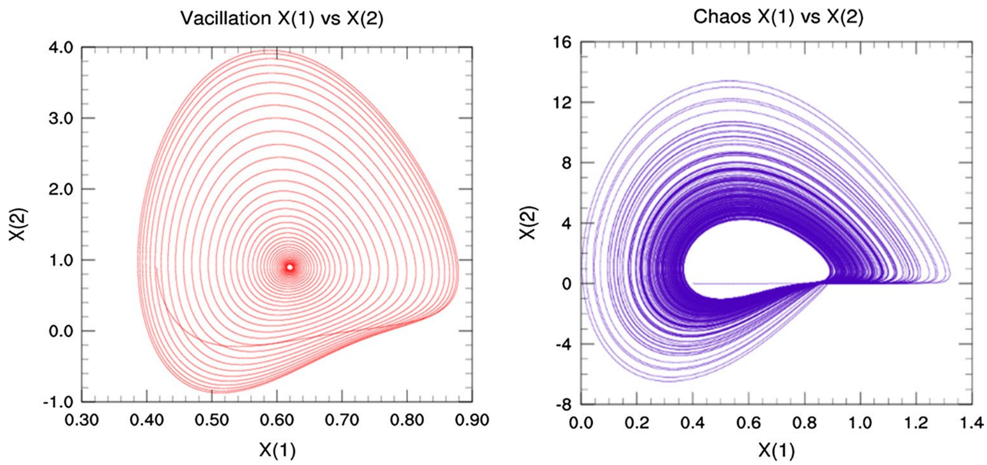

Fig. 1 Explosive baroclinic instability—vacillation on the left, chaos on the right (Fleming 2014)

The results for the 40,000 deterministic chaotic solutions were all different. The spread of solutions, using $X(3)$ as an example (the wave kinetic energy considered a proxy for storm intensity), provided a dynamic range. The maximum value of $X(3)$ within a chaos run was considered as a measure of the strength of that run. The average maximum $X(3)$ for all the runs was 18.95. The minimum and maximum of this $X(3)$ measure were 7.42 and 27.68—nearly a factor of four difference in magnitude.

This weather diversity would expand with the seasons with different heating characteristics. This weather variability would occur within any *climate-change* regime—warm or cold. However, there will never be runaway chaos as EBI is limited by the dynamics of the system (Fleming 2014).

Further changes in **H** and **D** were evaluated over a wide range. Large **H** and small **D** provide a fast system and small **H** and large **D** a sluggish system as anticipated. However, smaller values of **H** and **D**, as might be expected within an ice age, lean toward more chaos (Fleming 2015).

Does CO_2 have a role in causing *climate change*? Observations examined

The Earth was formed 4.6 billion years ago, and the atmosphere 600 million years later. The peak of the CO_2 degassing rate coincided with the maximum tectonic activity about 2.7 billion years ago—reaching a value of approximately 10,000 times the current atmospheric value of 400 ppmv (parts per million by volume). Water degassing occurred much earlier, but reached its peak about 2.5 billion years ago. There then began a systematic (but oscillating) decrease in atmospheric CO_2 as it combined with water to provide the hydration of rock forming minerals in the oceanic and continental Earth crust (Sorokhtin et al. 2007).

A comparison of CO_2 concentration in the atmosphere with some of the ice ages over time is presented from data shown in Fig. 2 (Plimer 2009). Atmospheric CO_2 continued to decrease (with oscillations up and down) until it had the value between 10 and 200 times today's concentration by 1.8 billion years ago (Kaufman and Xiao 2003).

Various Ice Ages are shown in Table 1 where the values of CO_2 concentration lie between the two extremes. Clearly, CO_2 values have no correlation with the ice ages.

Table 1 indicates CO_2 concentrations for the ice ages and the warm periods between them—where the surface temperature was estimated to be ~ 8 °C higher than today's average value. The Earth's albedo apparently decreased during the warm periods—the Sun's insolation has not changed over the past billion years (Sorokhtin et al. 2007).

The table illustrates no correlation of CO_2 and temperature. Why this is true must be looked at in detail and will be in "H_2O and CO_2 in the radiation package" section.

Ice cores with sufficient vertical resolution (time resolution) have provided 420,000 years of data from Antarctica indicating that the temperature changes preceded the corresponding CO_2 changes. An American team found the time lag (due to ocean mixing) of CO_2 behind temperature of several hundred years. The oceanic reservoir of CO_2 is far greater than that of the atmosphere. When the oceans are warm, they outgas CO_2, and when the oceans are cold atmospheric CO_2 dissolves into the oceans (Fisher et al. 1999).

A subsequent study in 2003 by a French team indicating that deglaciation was not caused by CO_2 which lagged the temperature by 200–800 years (Caillon et al. 2003). A third effort by Russian scientists arrived at the same conclusion, where the estimated delay was 500–600 years (Monin and Sonechkin 2005). This was claimed to be 420,000 years of data with undisputable evidence that CO_2 concentrations of the atmosphere are the effect of global temperature changes and not their cause (Chilingar et al. 2008).

Now consider the *climate change* over the past 11,500 years of the Earth's interglacial period. There exists

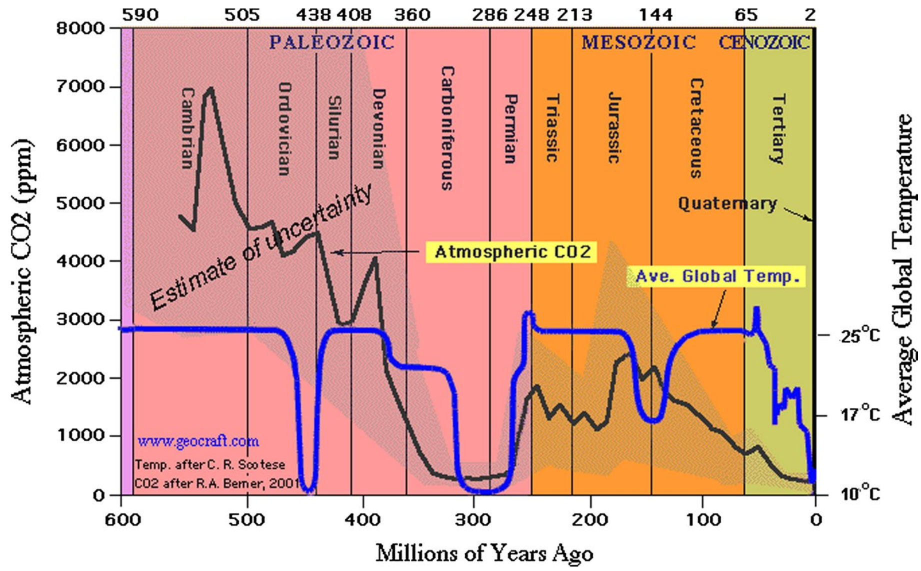

Fig. 2 Estimates of the CO_2 concentration and the Earth's surface temperature over time (Plimer 2009)

Table 1 Ice ages and intermediate warm periods from 65 to 850 million years ago

Various Ice Ages time (MYA)/name	CO_2 (ppmv)	Intermediate warm periods (MYA) $\Delta T = \sim 8$ °C	CO_2 (ppmv)
850–630/Cryogenic	~40,000	~480–600	4200
460–430/Andrean-Saharan	4000–4400	~360–420	3000
350–260/Karoo	370–400	~170–240	1200
160–120/Scutum-Crux	2000–2400	~50–100	1000

an excellent summary (Plimer 2009) of these alternating warm and cold periods. Only two of these are listed below.

Medieval Warming (900–1280) was a warm period where society thrived! The summers were long, the crops were plentiful. The population increased, cities grew, universities were established and cathedrals were built (Gimpel 1961).

The Little Ice Age (1300–1850) occurred in two major phases, with famine in Europe killing millions between 1690 and 1700 (Grove 1988). The Little Ice Age was initiated with what is called a "quiet Sun" a period of very few sunspots—referred to as a *Solar Minimum*. The Maunder Minimum was the most important (1645–1715).

Cosmic rays are star dust—mostly hydrogen protons from exploding stars. These enter the Earth's atmosphere when the Sun is "quiet"—the solar wind and its magnetic field are weak.

An isotope is produced from the normal light element of beryllium (normally with 4 protons and 5 neutrons) into beryllium-10—it is produced by cosmic rays as follows. A cosmic ray entering the atmosphere creates a shower of secondary cosmic rays, e.g., an energetic neutron. This collides with an oxygen atom, removing a neutron for beryllium to make beryllium-10 (4 protons and 6 neutrons). Be-10 has a half-life of 1.4 million years.

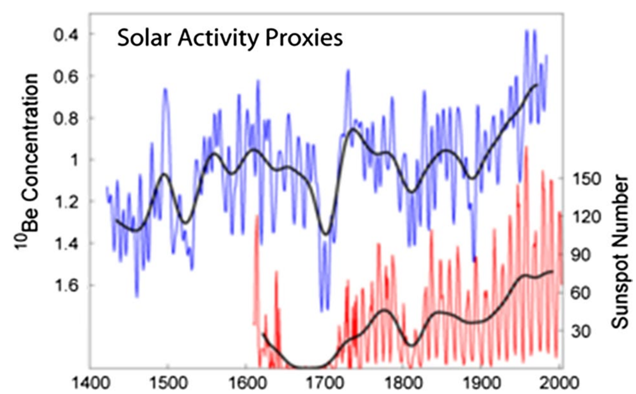

Fig. 3 Be-10 values with solar activity—sunspot numbers from Hoyt and Schatten (1998), Be-10 from Beer et al. (1994)

Figure 3 indicates Be-10 values are strong when cosmic rays are strong (when the Sun is weak)—note the strong values during the important Maunder Minimum of the Little Ice Age. Be-10 values have weakened considerably with the strong Sun during the *Modern Warming*.

Another proxy for solar activity involves cosmic ray interaction with nitrogen (N-14, normally 7 protons and 7 neutrons). In this case, the energetic neutron collides with nitrogen and the atom loses a proton and gains a neutron

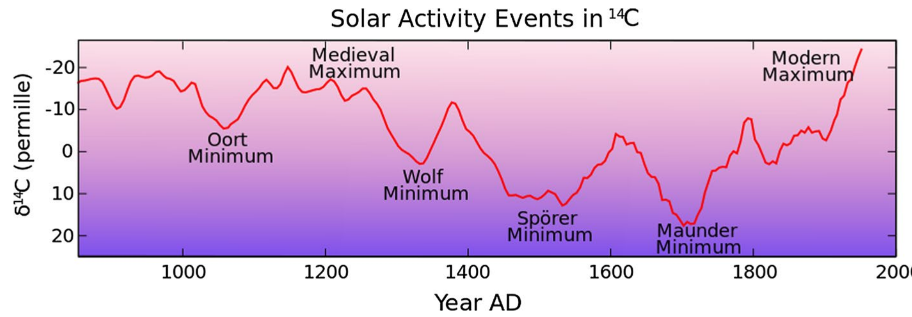

Fig. 4 Carbon-14 values with weak and strong solar activity (Plimer 2009 modified from his B&W version)

to become carbon-14 (6 protons and 8 neutrons). Normally the carbon atom is carbon-12 (6 protons and 6 neutrons). Figure 4 adapted from (Plimer 2009) indicates C-14 data are extremely small during the warm Medieval Warming and also in the Modern Warming since 1850. The C-14 values also have largest magnitudes at the sunspot minima.

The CO_2 concentrations have relatively little change over the interglacial period (see Fig. 2). A Greenland ice core provided the value 270 ppmv dated from 600 years ago (Neftel et al. 1983). The pre-industrial revolution estimate by several methods provides a narrow range of 270–290. Further detail in "Solar magnetic field/cosmic ray factors affecting climate change" section indicates no correlation of CO_2 with any of the climate changes observed and well documented during the 11,500 interglacial period.

Since the Little Ice Age, a strong Sun is revealed by both Be-10 and C-14 decreases. The total magnetic flux leaving the Sun (dragged out by the solar wind) has risen by a factor of 2.3 since 1901 (Lockwood et al. 1999). The strong solar magnetic field has shielded the Earth from cosmic rays and is the cause of the Modern Warming that has occurred through to the current time. This competing climate theory is from Svensmark and Friis-Christensen (1997).

The theory involves the interaction of the solar magnetic field with cosmic rays. When the solar magnetic field is strong, it acts as a barrier to cosmic rays entering the Earth's atmosphere, clouds decrease and the Earth warms. Conversely when the solar magnetic field is weak, there is no barrier to cosmic rays—they greatly increase large areas of low-level clouds, increasing the Earth's albedo and the planet cools. The solar magnetic field is generated by the solar dynamo with the principal cause being the angular momentum of the Sun's differential rotation (Charbonneau 2014). The Sun's equatorial region rotates faster—24 days, compared to the polar regions which rotate once in ~ 30 days. This solar dynamo accounts for the variability of the sunspot amplitudes and frequency changes.

There is another factor affecting the solar dynamo that occurs on a longer time scale. This is the Sun's motion about the center of mass of the solar system—the solar system barycenter (SSB). The position of the SSB is constantly changing primarily as a function of the mass of the Sun and the

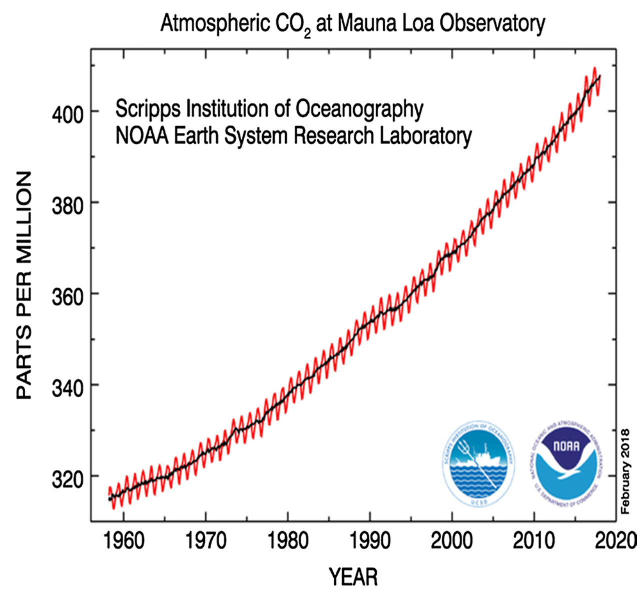

Fig. 5 CO_2 record from Mauna Loa from NOAA/CO_2 data/full record

four major planets (Sharpe 2008). The Sun's travel about the SSB adds its orbital angular momentum from that journey to its own rotational angular momentum so that both contribute to important changes in the Sun's magnetic field intensity. Details of all the factors that influence this solar magnetic field/cosmic ray interaction are described with references in "Solar magnetic field/cosmic ray factors affecting climate change" section.

This new climate-change theory competes with the CO_2 warming associated with the timing of the industrial revolution. The combination of both of these two solar magnetic field influences appears to be the cause of a twentieth-century cooling within the Modern Warming. Thus, it is imperative to consider the twentieth-century temperature record since the industrial revolution.

The World War II and postwar period was a time of tremendous industrial growth from 1940 to 1975 (Plimer 2009). Figure 5 indicates the modern CO_2 record from Mauna Loa which indicates the increased activity. However, there was a significant drop in temperature from coastal stations around the Arctic Ocean from 1940 to 1970 of 1.4 °C (Solomon

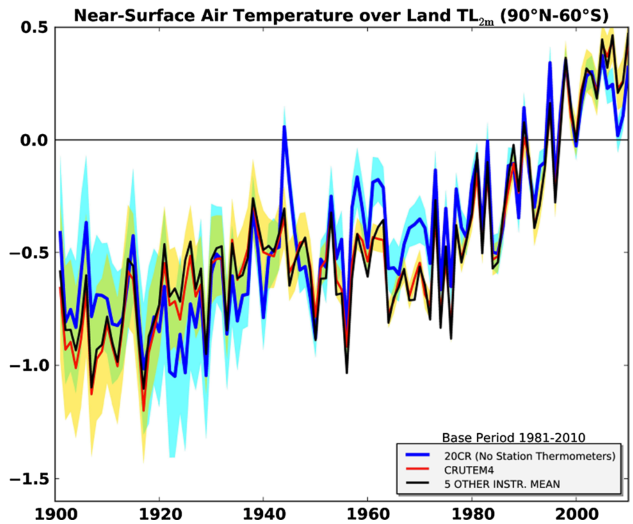

Fig. 6 Near-surface air temperature change in the twentieth century (see data sources in box within the figure)

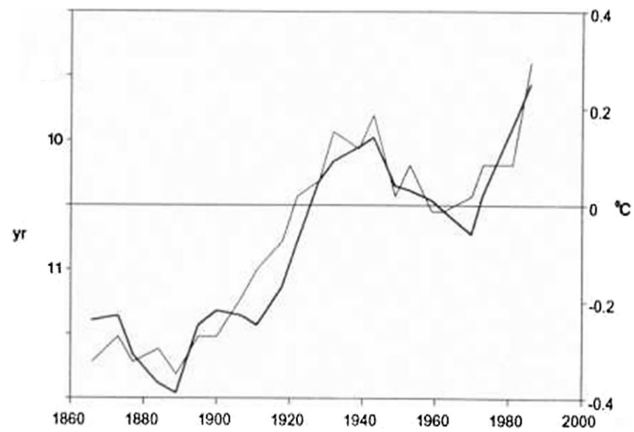

Fig. 7 Gleissberg record of LSC found in Landscheidt (2003)

2008). Also Fig. 6 shows a global cooling between 1940 and 1975 of surface temperatures over land (90 N–60 S) from three different records. The benchmark indicator for the CO_2 warming theory, the NOAA Mauna Loa carbon dioxide record, fails to indicate this 35-year period of cooling. There are two solar-related events that support this cool climate–change event.

In contrast to the smoothed decrease in the Be-10 data in Fig. 3 from the post Little Ice Age—a closer look at the background shows sharp spikes of significant Be-10 increases from 1900 to 1970 indicating increased cosmic rays. A second solar record below provides further evidence of this cool period.

The sunspot cycle has an average period of 11.2 years, but the length varies from 8 to 14 years. The length of a sunspot cycle (LSC) is an indicator of the Sun's eruptional activity. The Gleissberg (1965) cycle resulted from his smoothing of the time series of the length of the sunspot cycles (LSC) and a secular cycle of 80–90 years emerged.

Figure 7 is from Landscheidt (2003) where Gleissberg's smoothed data were displayed. The heavy line is the smoothed LSC line and the light line is the land air temperature in the Northern Hemisphere. The heavy line agrees very well with the temperature and also with the temperature record of Fig. 6 with the cooling from 1940 to 1975. It appears that the atmospheric temperature is oblivious to CO_2 concentration! Why? One must check the radiation calculations in "H_2O and CO_2 in the radiation package" section to see whether there is something special about the role of CO_2.

The source of the Earth's thermal blanket

The Sun's output has been steady for the last one billion years. Three processes have maintained the energy balance over that time period—any systematic deviation in either direction over such a long period of time would have made life on Earth impossible—a planet too hot (a burnt cinder) or too cold (a ball of ice).

These three processes are: radiation, latent heat release from condensation, and atmospheric convection. These all work together to heat the lower atmosphere, transfer heat upward and cool the upper atmosphere, and achieve radiative balance.

The Earth receives incoming solar radiation and radiates terrestrial longwave radiation. This radiant energy travels in waves at the speed of light (3×10^8 m/s in a vacuum). Details of radiation are described in "H_2O and CO_2 in the radiation package" section.

Water exists on Earth in three phases—solid, liquid and gas. The intermolecular forces in water molecules are decreased as energy (heat) is applied to the phases of water. The most important phase changes of water for the climate system are the Sun's energy (2500 J/g) evaporating water from the oceans, and then that energy being released as latent heat of condensation.

Convection is clearly the most important mechanism for transferring heat upward (Emanuel 1994). As hot air expands it becomes less dense and rises. Similarly, denser cooler air drops down and replaces the warmer air. This is a diabatic process as there is always some entrainment (conduction—molecular collisions exchanging heat—a minor process within a gas, but nevertheless present.)

Sorokhtin et al. (2007) have provided a way to quantify these processes in relative terms. Their procedure is clever and provides representative values for the three forces—at least in a space/time averaged sense. The values for the three processes are:

diabatic convection: 0.2394/0.3597 = 66.56%,
diabatic condensation of water vapor = 0.0896/0.3597 = 24.90%,
diabatic radiation (primarily H_2O and CO_2) = 0.0307/0.3597 = 8.54%.

These values are useful, but should not be taken too seriously—they are, at best, ensemble averages over space/time. Their sum may be close to 100%, but there can be significant variability among the processes. This diversity is assured by the chaotic nature of the atmosphere. The radiation component has the smallest percentage impact, but has an important day-to-day role in providing energy balance.

H_2O and CO_2 in the radiation package

Figure 8 is a visual of the spectrum of longwave radiation adsorbed and emitted from the Earth and its atmosphere. The abscissa represents wavelengths of radiation in microns

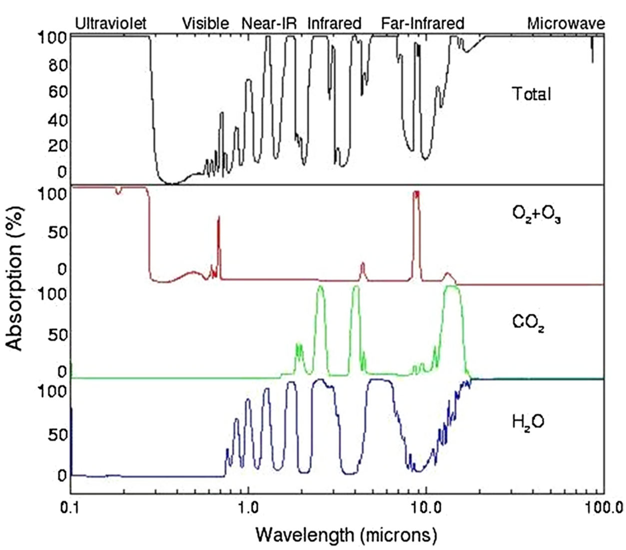

Fig. 8 Absorption spectrum for H_2O and CO_2 (Rothman et al. 2009)

(10^{-6} m or 10^{-4} cm and "microns" are shortened to μm). Incoming solar energy for climate is important in the short range of 0.1–2.0 μm—and for longwave terrestrial radiation the range is from 4.0 to 40 μm (Peixoto and Oort 1992).

Radiation interacts with matter on both the atomic and molecular level. Gases in atomic form adsorb and emit radiant energy in very narrow wavelengths that result from quantized changes in electronic states—called spectral absorption lines. Vibrational absorption occurs within a molecule due to the vibration of component atoms about their mean position within the molecule. Rotational absorption is due to the rotation of a molecule around its center of mass. The multiplicity of vibrational–rotational modes creates a complex irregular absorption spectrum with bands containing thousands of lines. The strongest of the H_2O lines have not the strength of the strongest of the CO_2 coefficients.

One can make a broad brush comparison of the relative roles of H_2O and CO_2 in the heating of the thermal blanket. The units on the coefficients in Table 2 are in m^2/kg. The comparison is for the level of the thermal blanket considered to be one km thick within the planetary boundary layer.

The concentration of CO_2 is considered to be uniform over the atmosphere at 400 ppmv. The concentration of water vapor varies from a maximum of 40,000 ppmv (Hong Kong) to the lowest measured value of 4 ppmv in the upper stratosphere. A value for water vapor at one km is estimated to be 11,000 ppmv, so the ratio of mass of H_2O/CO_2 at one km is approximately 11,000/400 = 27.5. Comparison of the absorption coefficients over the full range of 1.5–18 μm gave the result: $CO_2/H_2O = \sim 5.5$. Thus, water vapor dominates by the ratio of 27.5/5.5 = 5.

The CO_2 absorption coefficients obtained directly from the Pacific Northwest National Laboratory (Rothman et al. 2009) were 3,900,000 in number ranging from 1 to 40 μm. Based on the author's limited personal computer/software, only every 10th line was used bring the total down to 390,000. Table 3 indicates the values of those coefficients according to magnitude. The reduction was implemented so that the true maximum coefficient was used.

These two data sets are statistically equivalent. Table 3 indicates that the number of coefficients considered transparent $K < 1$ is 98%—and the maximum is the same in both data sets. The average value of each is virtually the same. In all

Table 2 Absorption coefficients for H_2O and CO_2 from Pacific Northwest National Laboratory/Rothman et al. (2009)

Band name	Range wavelength (μm)	Max value (m^2/kg)	Average value
H_2O Band 1	2.55–2.84	78.02 at 2.6705 μm	2.10
H_2O Band 2	5.00–7.10	82.83 at 5.9351 μm	2.10
H_2O window	8.0–16.0	1.2	0.0063
CO_2 window	5.0–13.0	0.06	0.0005
CO_2 Band 1	4.20–4.50	4596 at 4.2346 μm	68.4
CO_2 Band 2	13.61–16.00	596.1 at 14.98 μm	8.8

Table 3 CO_2 absorption coefficients from PNNL

CO_2 absorption coefficients (K)		390,000 lines	3,900,000 lines
Units are m^2/kg	1–40 μm	$K<1$ transparent	$K<1$: transparent
%Transparent		98.00	98.00
Maximum value		4596	4596
Average value		1.2503	1.2482
$K<0.0001$		228,424	2,284,198
$0.0001 \geq K<0.001$		102,982	1,029,996
$0.001 \geq K<0.01$		30,004	300,007
$0.01 \geq K<0.1$		11,994	119,933
$0.1 \geq K<1.0$		8811	88,201
$1.0 \geq K<10.0$		4438	44,289
$10.0 \geq K<100.0$		2695	26,853
$100.0 \geq K<1000$		544	5453
$K>1000$		108	1070
Total lines		390,000	3,900,000

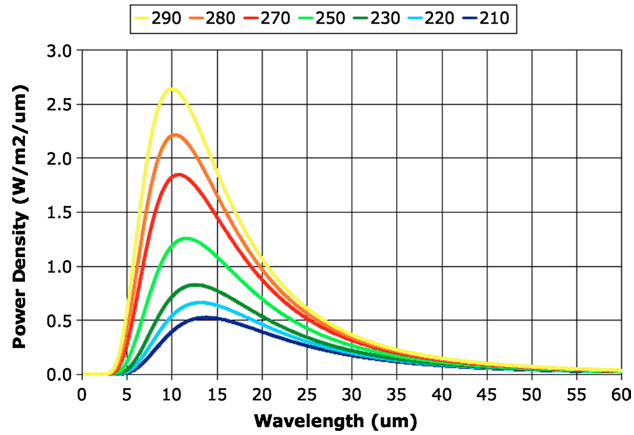

Fig. 9 Radiative power intensity expressed by Planck's equation (this plot by Hashemi 2010)

categories of the various magnitudes of the coefficients, the number in the data set with 390,000 coefficients is approximately 10% of the number in the larger data set.

The important equations for radiative transfer are Planck's equation for the intensity of radiation, and the integration of the Schwarzschild equation for net diffuse radiation. One can see Houghton (1985) and Liou (2002) for details. The equation is found in radiation texts and the curves below computed for values of wavelength (λ) and T.

The integration of the Schwarzschild equation is used in the computations below. The largest impact from level to level in this equation is the change in the intensity of the Planck equation (see Fig. 9) and note how it changes with temperature and wavelength). The formula is:

$$B(\lambda, T) = \left[2\Pi hc^2/\lambda^5\right]\left[\exp\left(ch/k\lambda T\right)-1\right]^{-1}$$

Consider the transfer of thermal infrared radiation emitted from the Earth and the atmosphere where a beam of intensity will undergo the *absorption* and *emission* processes simultaneously. The Schwarzschild equation for this process is: $\mathrm{d}I_\lambda/k_\lambda\rho\mathrm{d}s = -I_\lambda + B_\lambda(T)$; where the first term on the right-hand side denotes the reduction in radiant intensity due to absorption, whereas the second term represents the increase in radiant intensity arising from the blackbody emission of the material.

The atmosphere is considered to be in thermodynamic equilibrium and is plane parallel. A differential optical depth can be defined as $\mathrm{d}\tau = -k_\lambda(z)\rho(z)\mathrm{d}z$. The coordinates are below from Liou.

0	Z_∞	--- --- --- --- --- --- --- --- --- --- --- --- --- --- --- --- ---	T_∞	u_1	0
τ'	Z'	--- --- --- --- --- --- --- --- --- --- --- --- --- --- --- --- ---	T'	u'	P'
τ	Z	--	T	u	P
τ'	Z'	--- --- --- --- --- --- --- --- --- --- --- --- --- --- --- --- ---	T'	u'	P'
τ_S	0	____	T_S	0	P_S

The coordinate systems in τ, Z, u, T and P for IR radiative transfer are shown above. The path length (u) is for absorbing and emitting gases (they absorb and warm and emit and cool) defined for the surface upward. The total path length is defined as u_1. T_∞ and Z_∞ are temperature and height at the top of the atmosphere. The surface temperature $= T_S$. The surface pressure is P_S. Z is a reference level.

The Schwarzschild equation solution using the Liou notation above and equations of Houghton is: $F = -\int B(\lambda, T)(\mathrm{d}\tau^*)/\mathrm{d}u)\mathrm{d}u + \int B(\lambda, T)(\mathrm{d}\tau^*)/\mathrm{d}u)\mathrm{d}u$; the optical depth ($\mathrm{d}\tau^*$) is due to the radiation being diffuse rather than a parallel beam.

In the first integral, the integration proceeds *downward* along the optical path from the reference level (Z) with optical path u *downward* to the surface where the optical path = 0. In the second integral, the integration proceeds upward from the reference level (Z) with optical path u upward to the top of the atmosphere where the total optical path is u_1. Both integrals are positive, because of the convention that the path length is measured positive down and then positive up, respectively. The net flux at a level is the upward flux at the bottom of a layer minus the downward flux at the top of a layer.

Calculations begin with the CO_2 lines and coefficients in Band 1. The maximum coefficient in this band is quite large—the value of this coefficient $K_\lambda = 4596$ m^2/kg and occurs at the wavelength of $\lambda = 4.2346463$ µm. All the 390,000 lines are organized by increasing wavelength, paired with their surface absorbance coefficient. One starts with a formula for the lines. The number of lines displayed in this presentation will vary from 70,000 to 300,000. Many more runs were performed over a wide range of lines—all of these runs provided similar numbers with the same conclusion. Band 1 run uses the formula below with $J = 1$–70,001.

$\lambda = 1.0 + (J-1) * 0.00005 + 0.0346463$. This provides lines from 1.0 to 4.50346463 µm. The value of $J = 64{,}001$ provides a direct hit on the largest absorption coefficient at $\lambda = 4.2346463$. Every line in the formula is evaluated at every level (Δheight = 1 km) with the following steps for each line and level. Information for each level is saved going upward, then downward.

(1) The line is selected from the formula for $J = 1$–70,001.
Note that the only line guaranteed to be exact is $\lambda = 4.2346463$. Other lines may also be exact, but in any case they are extremely close and linear interpolation provides the proper coefficient.
(2) The standard temperature T at that height is selected for use in the Planck subroutine along with the wavelength to arrive at the proper Plank radiation intensity for that $B(\lambda, T)$.
(3) Rather than separate each reduction with height—i.e., the reduction in the Planck function $B_\lambda(\lambda, T)$, the reduction due to changes in the CO_2 density; and the reduction to the coefficient magnitude with temperature, one can obtain the same final answer by incorporating those changes into a single coefficient of reduced intensity (K_E). The first of the three steps is the Planck change with height: $K_E = K_\lambda \times [B(\lambda, T)/B(\lambda, T_{Surface})]$ [note the original surface K_λ is used for the first level (1 km)].
(4) The new K_E is further reduced by the density change in CO_2.
$K_E = K_E \times \rho(T, P)/\rho\ (T, P)_{Surface}$ where $\rho = P/1.889\ T$. [Where $P = \rho\ R\ T$, and R is for CO_2.]
(5) The new K_E is further reduced by the decreasing temperature with height as K_λ increases in line strength with height. $K_E = K_E \times (T/T_{Surface})$.
(6) The final step is to correct for the path length since the radiation is diffuse. Several options, see Houghton (1985) and Liou (2002), all produce similar results. The options ranged from (0.602 reduction for strong coefficients and 0.5 for weak) to 0.6 for all coefficients. Both Bands 1 and 2 calculations used $K_E = 0.6\ K_E$ for all the absorption lines.

Having performed all the steps above, the data are saved, checked and statistics determined for each level: including the percent transparent determined for all $K_E < 1$. Note that K in all the tables is K_λ at the surface and K_E for all other layers above the surface.

These results for Band 1 (Table 4) reveal several important points. The first is that 93.68% of the surface coefficients K_λ are transparent with values < 1—quite a large number. This is important as all the CO_2 molecules are influenced by all the coefficients. The derived coefficients of reduced

Table 4 Schwarzschild solution for Band 1: 1.0–4.5 µm

Lines Schwarzschild	70,001	70,001	70,001	70,001	70,001	70,001
K = coefficient	Surface	5 km	8 km	9 km	12 km	17 km
%Transparent	93.68	99.37	99.95	100	100	100
Max K	4596	60.582	5.104	0.6902	0.0240	0.0148
Average K	5.722	0.068	0.0124	0.0008	0.00003	0.00000005
$K < 0.0001$	26,410	58,947	64,542	65,619	68,328	70,001
$0.0001 \geq K < 0.001$	22,089	4352	1927	1589	1358	0
$0.001 \geq K < 0.01$	9236	2639	2093	2088	264	0
$0.01 \geq K < 0.1$	4567	1832	1160	568	51	0
$0.1 \geq K < 1$	3273	1787	243	137	0	0
$1 \geq K < 10$	1915	309	36	0	0	0
$10 \geq K < 100$	2002	135	0	0	0	0
$100 \geq K < 1000$	407	0	0	0	0	0
$K > 1000$	102	0	0	0	0	0

intensity are 100% transparent from 9 to 17 km. Despite the very powerful absorption coefficients in Band 1 (there were 102 values greater than 1000), the influence of the Planck function is very strong.

The influence of line shape (see references) was included in the above calculation. These are important only for *strong lines* and they were included only when K_E was > 50. Removing the line shape changed the numbers slightly, but not the result. Different diffuse radiation options were used and provided the same primary result—each option provided the same levels having 100% transparent values.

The most important difference for Band 2 is the longer wavelengths where the Planck differential with height is considerably less—as indicated in Table 5. Many runs were made over the Band 2. All the runs with various numbers of lines and over various ranges of lines gave essentially the same bottom line results. Thus, the decision was made to minimize space and display runs of simultaneously calculating Bands 1 and 2 for all wavelengths between 1 and 30 µm. Two runs were performed with 150,000 and 300,000 lines.

The temperature profile used for these calculations was that for the standard atmosphere, however, a very wide range of profiles scattered about that standard (some very stable, some very unstable) also produced the same upper-level transparency—all occurring first at 9 km.

These two Schwarzschild runs are shown together in Table 6—both runs give essentially the same results with 100% transparency at 9 km through 17 km. The maximum coefficient at 9 km is 0.69 in both cases. The CO_2 coefficients had > 95% of the surface coefficients already transparent. The maximum coefficient of reduced intensity K_E=0.69 at 9 km implies only a slight residual of heat available at that altitude—though the coefficient is virtually transparent. All the remaining smaller coefficients are transparent—also allowing heat to space un-impeded.

The volume of H_2O at the one km level alone is capable of absorbing all the available solar heat at the surface, and does absorb five times that of CO_2. All the heat adsorbed at the surface was fully redistributed vertically by all the molecules with the help of all the coefficients.

Table 5 Planck intensity: $B(\lambda, T)$ for the strongest coefficients in Bands 1 and 2

Height (km)	Temperature	$B(\lambda, T)/B(\lambda, T_0)$ $\lambda = 4.23466$	$B(\lambda, T)/B(\lambda, T_0)$ $\lambda = 14.9815$	CO_2 density $\rho(T)/\rho(T_0)$	T/T_0
0	288.15	1.0000	1.0000	1.0000	1.0000
1	281.65	0.7619	0.9235	0.9075	0.9774
3	268.65	0.4252	0.7791	0.7422	0.9323
5	255.76	0.2236	0.6466	0.6010	0.8872
7	242.65	0.1098	0.5265	0.4813	0.8421
9	229.65	0.0497	0.4192	0.3807	0.7970
11	216.15	0.0205	0.3251	0.2971	0.7519
13	203.65	0.0075	0.2443	0.2283	0.7067
15	190.65	0.0024	0.1768	0.1725	0.6616
17	177.65	0.0007	0.1220	0.1277	0.6165

Table 6 Schwarzschild runs: 1–30 µm with 150,000 and 300,000 lines

Lines Schwarzschild	150,000	150,000	150,000	300,000	300,000	300,000
K = coefficient	Surface	9 km	17 km	Surface	9 km	17 km
%Transparent	95.25	100	100	95.25	100	100
Max K	4596	0.690	0.001	4596	0.690	0.001
Average K	1.418	0.0009	0.000001	1.403	0.0009	0.000001
$K < 0.0001$	23,488	136,035	149,608	46,967	272,061	299,210
$0.0001 \geq K < 0.001$	89,475	6730	392	178,948	13,482	790
$0.001 \geq K < 0.01$	13,792	5706	0	27,554	11,399	0
$0.01 \geq K < 0.1$	8737	1204	0	17,505	2408	0
$0.1 \geq K < 1$	7381	325	0	14,769	650	0
$1 \geq K < 10$	5252	0	0	10,507	0	0
$10 \geq K < 100$	1489	0	0	2983	0	0
$100 \geq K < 1000$	359	0	0	717	0	0
$K > 1000$	27	0	0	50	0	0
Total lines	150,000	150,000	150,000	300,000	300,000	300,000

The solar input at the surface varies with cloud cover, and of course with the four seasons of the year as the Earth traverses its path about the Sun. Progressively warmer days in Northern Hemisphere summers are met with progressively cooler days in the Southern Hemisphere. The temperature of the thermal blanket varies accordingly. Adding passing clouds in some statistical way would lower the above numbers slightly, but not change the conclusion.

One can summarize these calculations as follows: whatever the "*climate-change regime,*" whatever surface heat from the Sun on any given day within that regime, that heat is fully absorbed and fully vertically redistributed throughout the troposphere—there is no propensity for CO_2 to store heat in a systematic way over time to produce a climate-change effect (as defined in the introduction).

Why does the integrated effect of CO_2 have so little effect on the total temperature profile? The reason is that the Planck function change with height (temperature) is very strong in reducing the intensity of those relatively few lines with large absorption coefficients. Another reason is that the longwave radiation is diffuse which depletes the intensity rapidly over distance. The diffuse nature of the radiation also leads to the fact that the *net radiation* for a given level (that sent upward at the bottom of a layer, minus that sent downward at the top of a layer) further reduces the adsorbed CO_2 radiation intensity.

Other so-called "greenhouse gases" (some with larger absorption coefficients, but all with significantly less concentration) have their intensity quickly transferred upward and depleted by the same strong Planck function intensity change that applies to CO_2 and H_2O.

From the historical record and from these calculations one sees that the CO_2 concentration had no impact on temperature. It contributes low-level heating and allows upper-level cooling for a zero net effect.

Similar calculations (not shown here) with the H_2O bands in Table 2 provided transparencies at even lower levels than CO_2 as expected from the smaller absorption coefficients. However, the cooling effect of water vapor may be just as great as CO_2 in the *upper levels* (though the concentration of H_2O is less) because of the water vapor continuum between 8 and 13 μm which collectively acts with stronger absorption than the individual lines in that spectral region (Stephens 1994).

Solar magnetic field/cosmic ray factors affecting *climate change*

The work of (Usoskin et al. 2007) provides a history of Grand Minima since 9500 BC. There have been 27 Grand Minima with various durations (from 30 to 110 years), with various time intervals between events. The summarized result from this work was a weak tendency for Grand Minima to cluster with a quasi-period of about 2400 years, and no clear periodicities were observed. There were not significant *climate-change events* with all of these Grand Minima. They were all tied to a special state of the solar dynamo, and (Charbonneau 2014) has expressed the fact that there is strong intermittency in the solar magnetic activity associated with the dynamo.

A significant improvement in determining which Grand Minima are important for *climate change* came with the work of Sharpe (2008) using Jet Propulsion Laboratory DE405 ephemeris data providing the results in Figs. 10 and 11. His C-14 data from Stuiver et al. (1998). The results confirm the reason for the Medieval Warming and the Little Ice Age (1300–1850) with its three separate Grand Minima (Spörer Maunder, and Dalton).

The synodic period (T_S—two successive conjunctions of the same bodies) of two planets 1 and 2 is given by $1/T_S = 1/T_1 - 1/T_2$ (with $T_1 < T_2$). The sidereal periods for Uranus and Neptune are 84.02 and 164.79 years, respectively. This gives $T_{UN} = 172$ years. This is the main driver seen in the angular momentum of the Sun about the SSB. The relationship of when a solar Grand Minima occurs always involves these four giant planets in their relationship with the Sun and as depicted in Fig. 11—Uranus, Neptune and Jupiter together and Saturn opposite the Sun. Type A events have a slightly stronger impact, but that detail is not relevant in the present discussion.

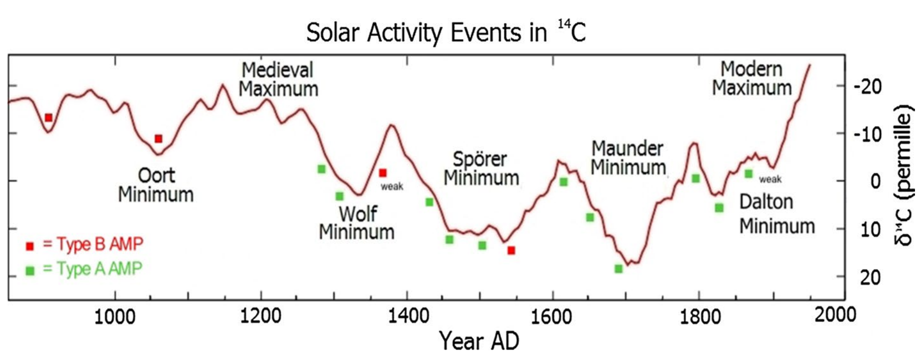

Fig. 10 Solar activity from Sharpe (2008) with his C-14 data from INTCAL98 (Stuiver et al. 1998)

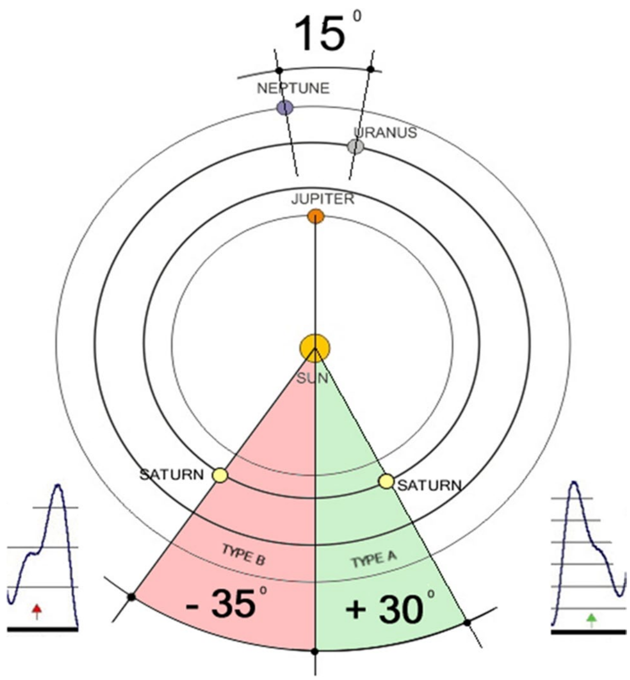

Fig. 11 Typical planetary positions for important grand minima (Sharpe 2008)

McCracken, et al. (2014) extended Sharpe's results back through the last 9400 years. The data sources for cosmic rays were the cosmogenic radionuclides Be-10 and C-14 from ice core records and tree rings. The data over the entire record confirms Sharp's results, and their statistical analysis found periodicities near 350, 510 and 710 years which closely approximate integer multiples of half the T_{UN} synodic period: $T=(T_{UN}/2)\ N$ years with $N=4$, 6, and 8. Using combinations of these periods one could approximate the transition between the various warm and cold periods observed in the past few 1000 years.

The range of the Sun's orbital angular momentum about the SSB varies from near zero to only 25% of the Sun's differential angular momentum driving the solar dynamo (Landscheidt 2003). Thus, the strength of the solar dynamo can outweigh the effect of the Sun/planet positions. Nevertheless, these results over this along period strongly suggest that the solar magnetic field/cosmic ray interaction is the primary cause of major climate-change events over the past 9400 years of the interglacial period.

The 35-year cool period within the current Modern Warming was an example where the Gleissberg cycle imposed only a modest impact on the existing strength of the magnetic field that was in place. The current Modern Warming will continue until the strength of the Sun's magnetic field declines.

Finally, there is the impact of cosmic ray intensity! Massive bright blue stars populate the rotating spiral arms of the Milky Way Galaxy. These massive stars have short lives. Small stars like the Sun live long enough to orbit around the center of the Galaxy many times. The journey about the Milky Way Galactic Core takes approximately 230 million years (Svensmark and Calder 2007). The solar system moves faster than the rotation of the spiral arms; thus, it is repeatedly running through the arms. The spiral arms contain many cosmic rays!

The length of this manuscript does not allow a further summary of that activity, but the reader will find that the Svensmark and Calder (2007) reference will take one over that journey, observing that all the Earth's major ice ages can be attributed to the Sun's magnetic field/cosmic ray interaction.

Summary

There is no correlation of CO_2 with temperature in any historical data set that was reviewed. The *climate-change* cooling over the 1940–1975 time period of the Modern Warming period was shown to be influenced by a combination of solar factors.

The cause of the Medieval Warm Period and the Little Ice Age *climate changes* was the solar magnetic field and cosmic ray connection. When the solar magnetic field is strong, it acts as a barrier to cosmic rays entering the Earth's atmosphere, clouds decrease and the Earth warms. Conversely when the solar magnetic field is weak, there is no barrier to cosmic rays—they greatly increase large areas of low-level clouds, increasing the Earth's albedo and the planet cools. The factors that affect these *climate changes* were reviewed in "Solar magnetic field/cosmic ray factors affecting climate change" section.

The calculations of "H_2O and CO_2 in the radiation package" section revealed that there is no net impact of CO_2 on the net heating of the atmosphere. The received heat is simply redistributed within the atmospheric column. This result is consistent and explains the lack of CO_2 correlations with observations in the past.

The current Modern Warming will continue until the solar magnetic field decreases in strength. If one adds the 350-year cycle from the McCracken result to the center of the Maunder Minimum which was centered in 1680, one would have a Grand Minimum centered in the year 2030.

Size constraints limited this review to a proper finish in providing more details about the climate theory of Svensmark, in particular, about the details of cloud formation and the precise timing of the ice ages. However, the reader can profit by reading (Svensmark and Calder 2007).

CO_2 is a valuable asset: providing the input to the plant world for the food all creatures require, and providing fresh oxygen for every breath inhaled by animals and mankind.

Hundreds of articles reveal the benefits of increased CO_2 under various environmental conditions. Examples include net productivity with greater water-use efficiency (Kimball 1983), and greater productivity even under conditions of chilling stress (Schwanz and Pelle 2001). Any greater CO_2 resource in the future will prove valuable when the Earth cools again.

References

Beer J, Baumgartner ST et al (1994) Solar variability traced by cosmogenic isotopes. In: Pap JM, Fröhlich C, Hudson HS, Solanki SK (eds) The sun as a variable star: solar and stellar irradiance variances. Cambridge University Press, Cambridge, pp 291–300

Caillon N, Severinghaus JP et al (2003) Timing of atmospheric CO_2 and Antarctic temperature changes across Termination III. Science 299:1728–1731

Charbonneau P (2014) Solar dynamo theory. Annu Rev Astron Astrophys 52:251–290

Chilingar GV, Sorokhtin OG, Khilyuk L, Gorfunkel MV (2009) Greenhouse gases and greenhouse effect. Environ Geol 58:1207–1213

Emanuel KA (1994) Atmospheric convection. Oxford University Press, New York, p 580

Fisher H, Wahlen M, Smith J, Mastroianni D, Deck B (1999) Ice core records around the last three glacial terminations. Science 283:1712–1714

Fleming RJ (2014) Explosive baroclinic instability. J Atmos Sci 71:2155–2168

Fleming RJ (2015) Analysis of the SDE/Monte Carlo approach in studying nonlinear systems. Lambert Academic Publishing, Saarbrucken, p 136

Gimpel J (1961) The cathedral builders. Grove Press, New York

Gleissberg W (1965) The eighty-year solar cycle. J Br Astron Assoc 75:227–231

Grove JM (1988) The little ice age. Methuen Press, London

Hashemi K (2010) http://homeclimateanalysis.blogspot.com

Houghton GH (1985) Physical meteorology. MIT Press, Cambridge

Hoyt DV, Schatten KH (1998) Group sunspot numbers: a new solar activity reconstruction. Part 1. Sol Phys 179:189–219

Kaufman AJ, Xiao S (2003) High CO_2 levels in the Proterozoic atmosphere estimated from analysis of individual microfossils. Nature 425:279–282

Kimball BA (1983) Carbon dioxide and agricultural yield: an assemblage and analysis of 430 prior observations. Agron J 75:779–788

Landscheidt T (2003) New little ice age instead of global warming. Energy Environ 14:327–350

Liou KN (2002) An Introduction to atmospheric radiation. Academic Press, London

Lockwood R, Stamper R, Wild MN (1999) A doubling of the sun's coronal magnetic field during the past 100 years. Nature 399:437–439

McCracken KG, Beer J, Steinhilber F (2014) Evidence for planetary forcing of the cosmic ray intensity and solar activity throughout the past 9400 years. Sol Phys. https://doi.org/10.1007/s11207-014-0510-1

Monin AS, Sonechkin DM (2005) Climate fluctuations based on observational data: the triple sun cycle and other cycles. Nauka, Moscow, p 191

Neftel AH, Oeschger J, Schwander J, Stauffer B, Zumbrunn R (1983) Ice core sample measurements give atmospheric CO_2 content during the last 40,000 years. Nature 295:220–223

Peixoto JP, Oort AH (1992) Physics of climate. American Institute of Physics, New York, p 522

Plimer I (2009) Heaven and Earth: global warming: the missing science. Quartet Books, Limited, London, p 503

Rothman LS et al (2009) The HITRAN 2008 molecular spectroscopic database. J Quant Spectrosc Radiat Transf 110:139–204 (**data provided by Pacific Northwest National Laboratory**)

Schwanz P, Pelle A (2001) Growth under elevated CO_2 ameliorates defenses against photo-oxidation stress in Poplar (Populous alba_x tremolo). Environ Exp Bot 45:45–53

Sharpe GJ (2008) Are uranus and neptune responsible for solar grand minima and solar cycle modulation? First published on line at http://www.landscheidt.info. arxiv.org/ftp/arxiv/papers/1005/1005.5303.pdf

Solomon L (2008) The deniers. Richard Vigilante Books, 239 pp. Page 77 has figure from S. Akasofu, Dir. of Intl. Arctic Research Center indicating the temperature drop as stated from a Russian source, but the published reference appeared to have the wrong year

Sorokhtin OG, Chilingar GV, Khilyuk LF (2007) Global warming and global cooling: evolution of climate on Earth. Elsevier, Amsterdam, p 313

Stephens GL (1994) Remote sensing of the lower atmosphere. Oxford University Press, New York, p 523

Stuiver MP, Reimer J, Bard E, Beck JW, Burr GS et al (1998) INTCAL98 radiocarbon age calibration, 24,000–0 cal BP. Radiocarbon 40:1041–1083

Svensmark H, Calder N (2007) The chilling stars: a cosmic view of climate change. Icon Books Ltd, Thriplow, p 268

Svensmark H, Friis-Christensen E (1997) Variation of cosmic ray flux and global cloud coverage: a missing link in solar-climate relationships. J Atmos Sol Terr Phys 59:1225–1232

Thompson PD (1987) Large-scale dynamic response to differential heating: statistical equilibrium states and amplitude vacillation. J Atmos Sci 44:1237–1248

Usoskin I, Solanki S, Kovaltsov G (2007) Grand minima and maxima of solar activity: new observational constraints. Astron Astrophys 471:301–309

Webster P, Keller JL (1975) Atmospheric variations: vacillation and index cycles. J Atmos Sci 32:1283–1300